

## CLIMATOLOGY

## Impact of current and warmer climate conditions on snow cover loss in burned forests

Arielle Koshkin<sup>1\*</sup>, Adrienne M. Marshall<sup>1</sup>, Karl Rittger<sup>2</sup>

Wildfires are increasingly burning in snow-dominated watersheds and can alter snowmelt dynamics. However, the spatial variability of snow cover loss in burned forests has been under characterized. Here, we use remotely sensed snow data to show that, under average winter conditions, snow melts earlier in the first year postfire in 99% of the snow zone. Postfire snow cover loss is more extreme in relatively low-elevation, warm environments compared to that in high-elevation, cold regions. Under +2°C of warming, 73% of the snow zone would experience more extreme earlier postfire snowmelt compared to historically average conditions. Regions with the largest shift earlier in postfire snowmelt timing under average climate conditions also have the largest shift earlier in postfire snowmelt under +2°C warming. The spatial variability in postfire snowmelt timing and exacerbated impact in projected warmer winters affect ecosystem water availability, snow albedo feedbacks, and snowmelt runoff forecasting essential to water resource management.

## INTRODUCTION

In snow-dominated regions globally, mountain snowpacks are a vital water resource for recharging aquifers and sustaining streamflow into the drier summer months (1). Snowmelt timing and magnitude are major controls on reservoir storage for municipal water supply, agricultural use, hydroelectric power generation, and flood control (2–4). In the western US, snowmelt-derived runoff from mountainous regions contributes up to 70% of total annual flow (5). However, with projected climate warming, western US snowpacks are predicted to decline by 40 to 75% by 2100 under high emissions climate scenarios (6, 7), with substantially shorter snow cover duration in observations (8, 9) and projections (10–12). Meanwhile, warmer summer temperatures and increased aridification are escalating water demands across the western US (13). Given these strains on snow-derived water systems, our understanding of snowmelt timing is essential to managing snow-derived water resources. Currently, no spaceborne sensor can quantify snow water equivalent accurately. Yet, snow cover can be mapped daily, allowing for spatially complete observations of annual snow disappearance date (SDD).

Simultaneously, wildfires are increasing in frequency, size, duration, and intensity (14). Fire is advancing to higher elevations, driven by warming (15), drier summers (16, 17), and earlier spring snowmelt timing (18). As a result, fires are more often burning in areas where precipitation typically falls as snow. In 2020 and 2021, satellite-observed wildfire activity in the seasonal snow zone (i.e., areas with persistent winter snowpacks) in California was nearly 10 times greater compared to the 2000 to 2019 period (19). Between 1984 and 2017, the area of western forests burned in the seasonal snow zone increased by up to 9% annually (19–21). The largest relative increase in area burned since 1984 has occurred above 2500 m, well into the seasonal snow zone in the western US (15).

In the aftermath of wildfires in the seasonal snow zone, the snow energy balance is altered, changing the snowpack's potential to sustain water storage throughout the winter. Snow albedo substantially modifies net shortwave radiation, a major contributor to the snowpack

energy balance, and, therefore, affects snowmelt magnitude and timing (22). In a postfire environment, burned vegetation and trees shed black carbon and charred woody debris onto the snow surface, decreasing the snow albedo (20, 23). With decreased albedo, the snowpack absorbs more energy and therefore melts earlier (21, 23–25).

However, postfire snowpack energy and mass balance are also influenced by tradeoffs between decreased canopy interception and increased net shortwave radiation (26, 27). In an unburned forest, canopy interception can reduce snow accumulation by up to 40% (28–30). Trees in an unburned forest also emit longwave radiation (29) and decrease incoming shortwave radiation (31, 32). When the canopy is removed, longwave radiation and snow interception might, therefore, decrease even as incoming and net shortwave radiation increases. Canopy removal could also increase latent and sensible heat fluxes by increasing wind speed at the snow surface (33, 34).

Climate also likely affects snow sensitivity to burned conditions: Colder winter air temperatures can yield snowpacks with higher cold content (the amount of energy required to melt a snowpack) throughout the winter, providing a higher energy threshold needed to melt the snow (35). High cold-content snow also has slower grain size growth, leading to sustained higher albedo (36). These cold snowpacks could, therefore, be less susceptible to modest changes in energy balance from postfire net shortwave radiation changes (19). Different postfire energy balance contributors could also vary in their importance over the years following fire as forests shed less black carbon and begin to regrow. The net consequences for mass and energy fluxes in burned forests, therefore, likely vary in both space and time and depend on both weather and climate conditions.

While some previous studies have found that SDD occurs earlier in postfire environments, these studies typically focus on one to three fires in similar regions (19, 27, 37–39). Those studies that have taken a larger scale approach have leveraged the western US-wide Snow Telemetry (SNOTEL) network of snow pillows to investigate regional-scale differences in postfire impacts on snow (40, 41). However, because SNOTEL sites are often placed in canopy gaps and are limited to point data, they do not fully capture the heterogeneity of snowpack evolution across a landscape (42). Previous studies have estimated postfire SDD advances ranging from 4 to 23 days using field observations and SNOTEL locations (14). Reasons for this

Copyright © 2025 The Authors, some rights reserved; exclusive licensee American Association for the Advancement of Science. No claim to original U.S. Government Works. Distributed under a Creative Commons Attribution NonCommercial License 4.0 (CC BY-NC).

Downloaded from <https://www.science.org> on October 16, 2025

<sup>1</sup>Hydrologic Science and Engineering, Colorado School of Mines, Golden, CO, USA.

<sup>2</sup>Institute of Arctic and Alpine Research, University of Colorado, Boulder, CO, USA.

\*Corresponding author. Email: akoshkin@mines.edu

variability have not yet been well explained, and remotely sensed data and modern statistics have been underutilized to tackle the problem of large-scale variability of snowpack change after fire.

Here, we provide a western US–wide analysis of wildfire impacts on SDD. We ask: (i) How does postfire change in SDD vary regionally, and what variables drive these discrepancies? (ii) How long do postfire impacts persist on SDD? (iii) What role does climate play in postfire SDD changes, and to what extent might climate warming exacerbate or mitigate postfire SDD changes? We evaluate SDD change based on the year since fire; elevation; and climate variables including solar radiation, winter average temperature, and seasonal snowfall (43).

We apply two complementary statistical approaches to enhance confidence and assess significance of our results: In the first, we fit linear regressions (LRs) to paired burned and neighboring unburned pixels, estimating SDD as a function of climate inputs, and infer the effect of fire based on the difference in residuals in the postfire period in burned compared to unburned pixels. In the second, we use an additive model fit over the western US to estimate SDD as a nonlinear function of annual climate conditions, topography, location, and burn. SDD is observed using a spatially and temporally complete (STC) dataset based on the MODIS (Moderate Resolution Imaging Spectrometer) Snow Covered Area and Grain-size (STC-MODSCAG), a daily fractional spectral mixture model derived from MODIS Terra surface reflectance from water year 2002 to 2022 (44, 45).

## RESULTS

### Year since burn and elevation influence on $\Delta$ SDD

SDD is highly spatially variable (Fig. 1A), driven by the heterogeneity of elevation, winter temperatures, winter solar radiation, and estimated snowfall across the western US (Fig. 1, B to E). To assess the postfire change in SDD ( $\Delta$ SDD) on a pixelwise basis, we estimated annual prefire SDD as a linear function of average winter temperature and estimated total seasonal snowfall for all years before the fire. We fit separate models for each pixel that burned between 2010 and 2021 [average coefficient of determination ( $R^2$ ) = 0.46]. SDD was then predicted for every water year (WY) for each pixel in the time series, including the postburn years. For each burned pixel, we identified the closest unburned pixel with similar characteristics and fit the same model over the prefire period (average  $R^2$  = 0.47). We then used these fitted linear models to predict SDD in the postfire period and calculated the difference between the postfire predictions and observations each year. The effect of fire on SDD based on LR ( $\Delta$ SDD<sub>LR</sub>) was estimated as the difference in postfire prediction errors between burned and unburned pixels. Negative  $\Delta$ SDD<sub>LR</sub> values indicate earlier SDD following a fire.

Fire had the largest effect at low elevations and in the first 5 years postfire (Fig. 2A). In the first winter following a fire,  $SDD_{LR}$  advanced by a mean of 3.3 [confidence interval (CI), 3.19 to 3.40 days] days across all elevations. These effects varied spatially, with 60% of burned pixels having earlier  $SDD_{LR}$  in the first year postfire. Mapped

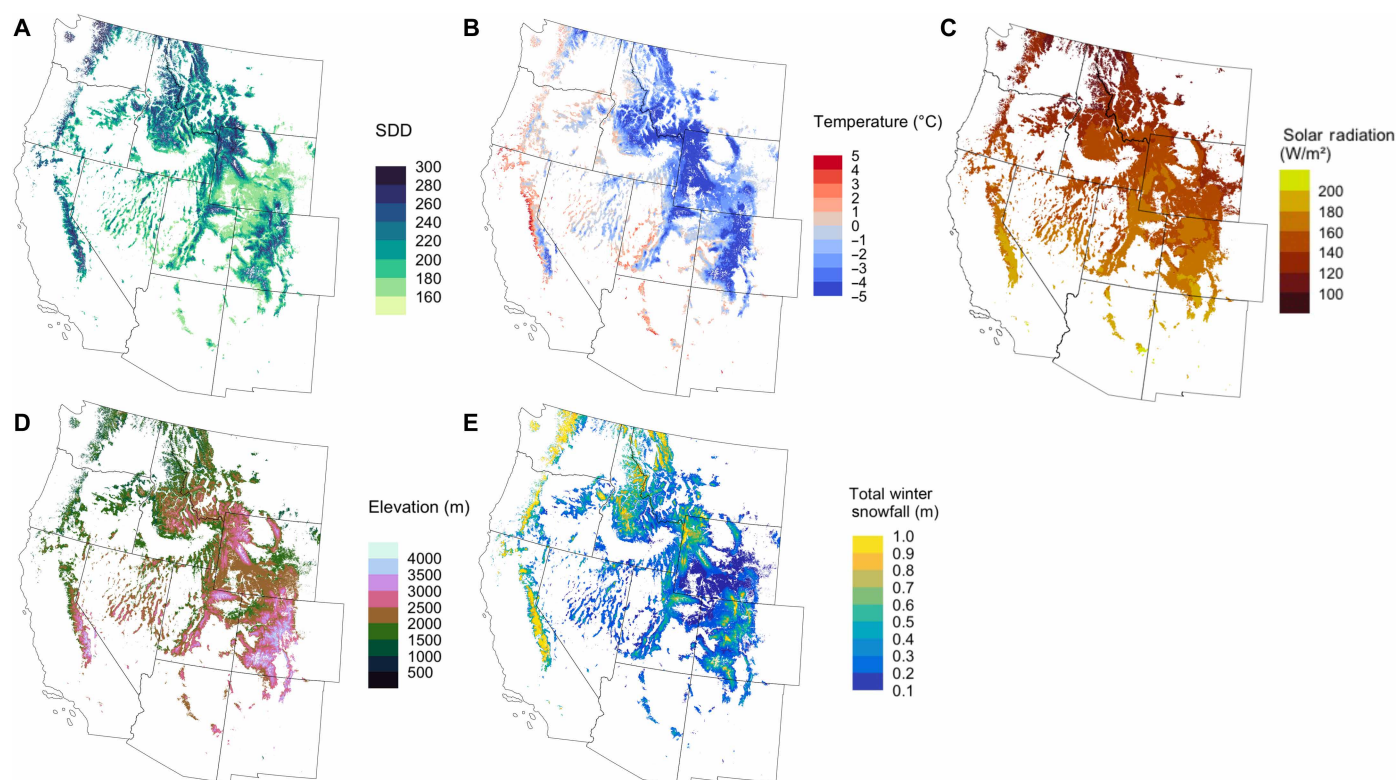


**Fig. 1. Spatial distribution of variables used to predict SDD.** (A) Mean SDD calculated from STC-MODSCAG. (B) Mean winter temperature (December to April) calculated from gridMet. (C) Mean winter solar radiation (December to April) sourced from gridMet and topographically corrected. (D) Elevation derived from Shuttle Radar Topography Mission. (E) Mean estimated annual snowfall calculated from gridMet for days with a mean temperature below 1°C. All means were calculated over 20 years from WYs 2002 to 2022.

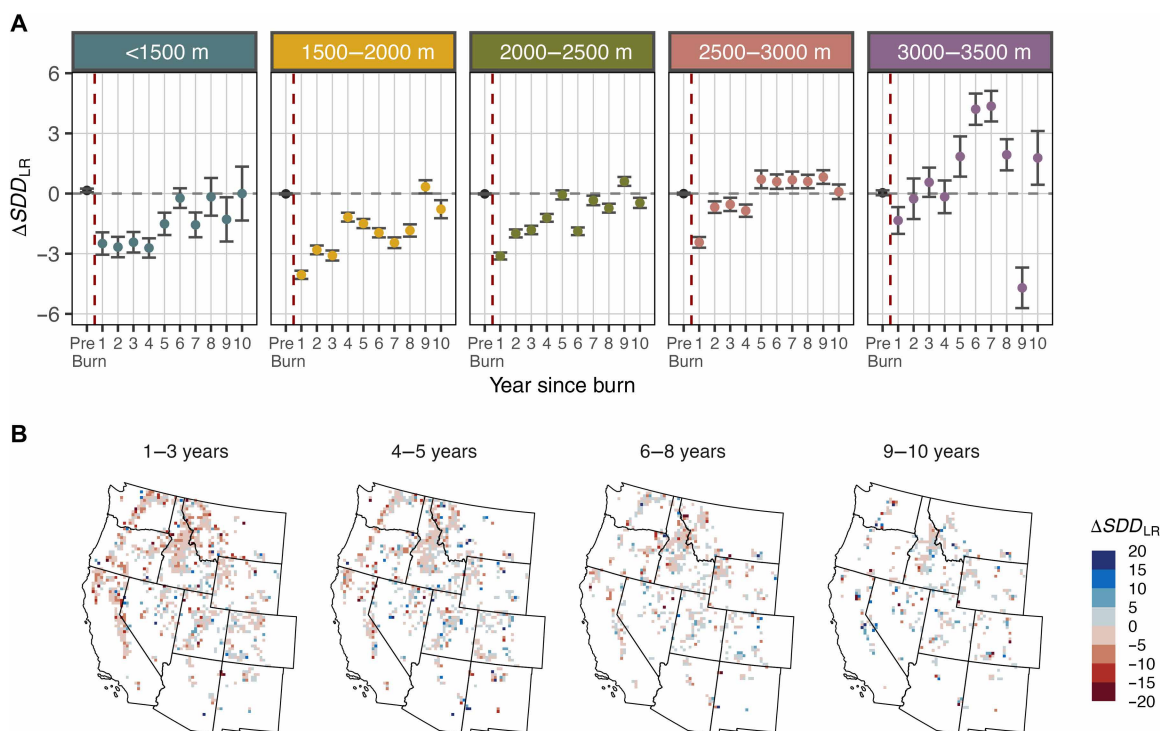


**Fig. 2. Estimates of  $\Delta SDD_{LR}$  by elevation and year since burn.** (A) Points indicate the mean  $\Delta SDD_{LR}$ , and bars indicate the 95% confidence intervals (CIs) for each winter since the burn. Year 1 is the first winter after the fire. (B) Maps of  $\Delta SDD_{LR}$  by year since burn. These data points were resampled to a coarser resolution to improve the clarity of the figure.

values indicated that, in the first year postfire,  $\Delta SDD_{LR}$  was the most negative across Northern California, the Pacific Northwest, and Idaho, with more positive  $\Delta SDD_{LR}$  values in Colorado and Utah (Fig. 2B). Below 2000 m,  $\Delta SDD_{LR}$  was a mean of 3.8 days earlier (CI, 3.62 to 3.97 days) 1 year postfire. Above 3000 m and below 1500 m, relatively wide CIs could be due to wider variety in effects or the smaller sample sizes at these elevation extremes (table S1).

Fire effects declined over time and started to show signs of recovery at mid-elevations: By 10 winters postfire, SDD only advanced 0.4 days earlier across all elevations, indicating that, in many cases, the effect of fire diminished over that period (Fig. 2). Above 1500 m, the  $\Delta SDD_{LR}$  was positive by five to nine winters following the fire, but, at high elevations (above 3000 m), this recovery period was as short as two winters postfire. At mid to high elevations (>2500 m), CIs were consistently above zero by five winters postfire, indicating that fire predominantly delays SDD at the highest elevations (Fig. 2A). Low elevations (<1500 m) did not show strong evidence of recovery until about eight winters postfire.

### Solar radiation and temperature effects on $\Delta SDD$

The magnitude of  $\Delta SDD$  estimated using either method varied with elevation and climate (Fig. 3). Positive  $\Delta SDD_{LR}$  values emerged at higher elevations, 5 to 10 years after a fire, especially in moderate- to high-solar-radiation conditions (Fig. 3A). The  $\Delta SDD_{LR}$  at moderate to high elevations under high-solar conditions became positive after four winters, while it took 10 winters for  $\Delta SDD$  to approach zero under low-solar conditions at low to mid elevations (Fig. 3A). Low elevations and the first 4 years following fire have relatively homogeneous  $\Delta SDD_{LR}$  estimates indicating 0 to 5 day earlier SDD.

In addition to the regression-based results, we fit an additive model across the western US to provide a more generalized assessment of

fire effects on snow, rather than estimating pixel-specific effect sizes. In this model, SDD was estimated as a nonlinear function (using thin-plate splines and tensor terms) of years since burn, spatial coordinates, elevation, winter temperature, snowfall, and shortwave radiation, with the effects of temperature and shortwave radiation fit separately for burned and unburned pixels. The model form was selected to minimize the root mean square error (RMSE) of a 10-fold cross-validation and avoid spatial patterns in the residuals.  $\Delta SDD$  in the additive model ( $\Delta SDD_{AM}$ ) is estimated by making model predictions for given climate conditions for hypothetical burned and unburned cases and subtracting the predicted SDD values for each pixel. Model results indicated that, under average burned or unburned conditions, SDD persisted latest in low to moderate solar conditions with cool temperatures, demonstrating the influence of both incoming shortwave radiation and temperature on snowmelt timing (Fig. 3, B and C). Inferred burn effects in the first year postfire were qualitatively similar to those of the LR approach, with the largest postfire  $\Delta SDD_{AM}$  in warmer temperatures and relatively low-solar-radiation conditions (Fig. 3D). Cold and sunny conditions allowed snow to persist longer in burned areas compared to unburned areas (Fig. 3D). Despite qualitative similarities between statistical approaches, the effect sizes estimated using the AM were larger than those estimated with the LR approach (Fig. 3, A and D).

### Regional variation in $\Delta SDD$ under historical climate variability

To understand how interannual climate variability and climate change could alter  $\Delta SDD$ , we used the additive model to examine predicted SDD in hypothetical burned and unburned conditions for a climatologically average winter for the first winter following the fire (Fig. 4A). Under these average historical climate conditions, snow in

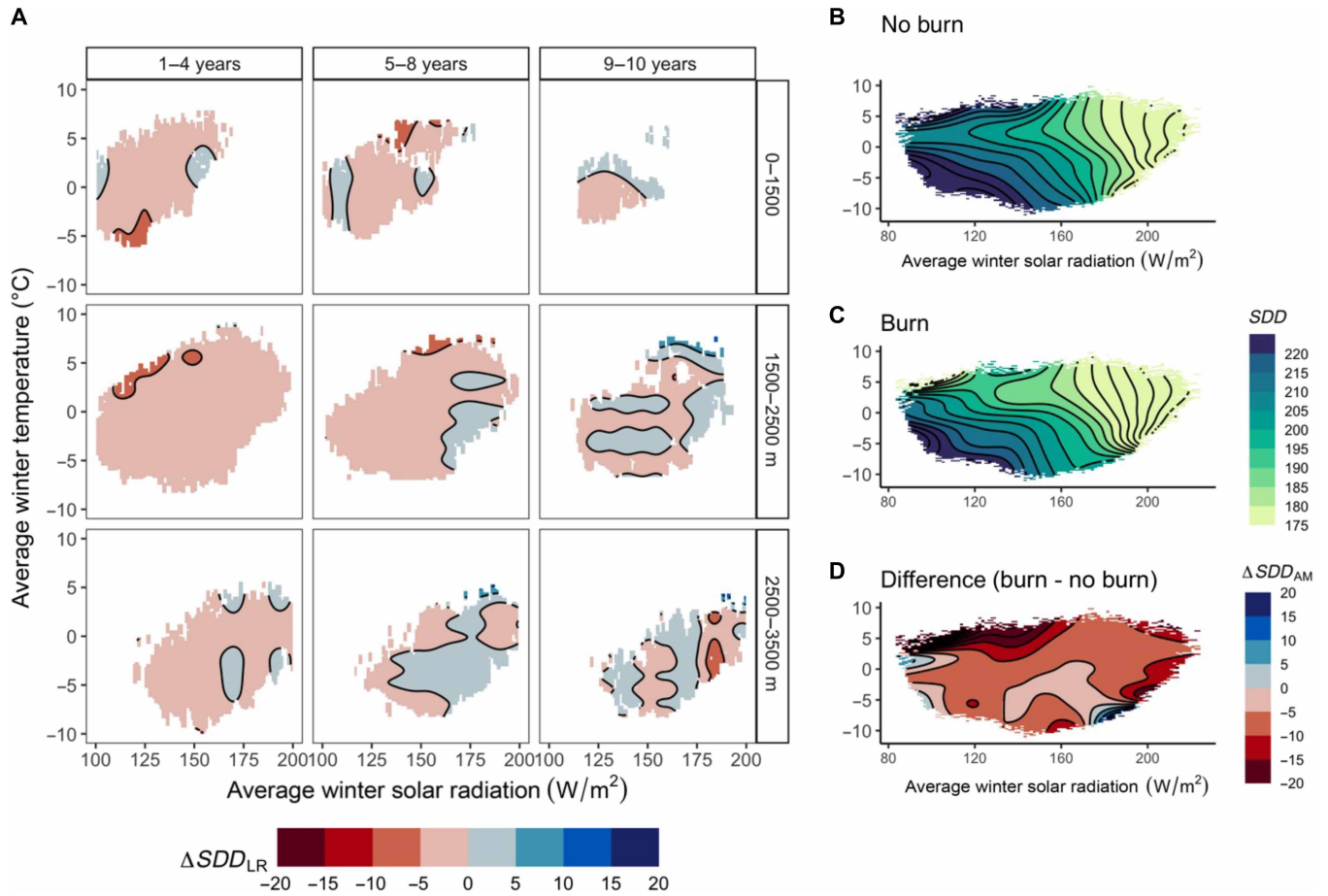


**Fig. 3. Modeled winter temperature and solar radiation effects on  $\Delta SDD_{LR}$  and  $\Delta SDD_{AM}$  to facilitate comparison among the two methods.** (A)  $\Delta SDD_{LR}$  estimated as a function of mean winter temperatures and mean winter solar radiation across elevation bands and years since fire in the LR. (B) SDD in unburned and (C) burned pixels 1-year post fire across the western US using the additive model (AM). (D)  $\Delta SDD_{AM}$  as a function of winter temperature and solar radiation.

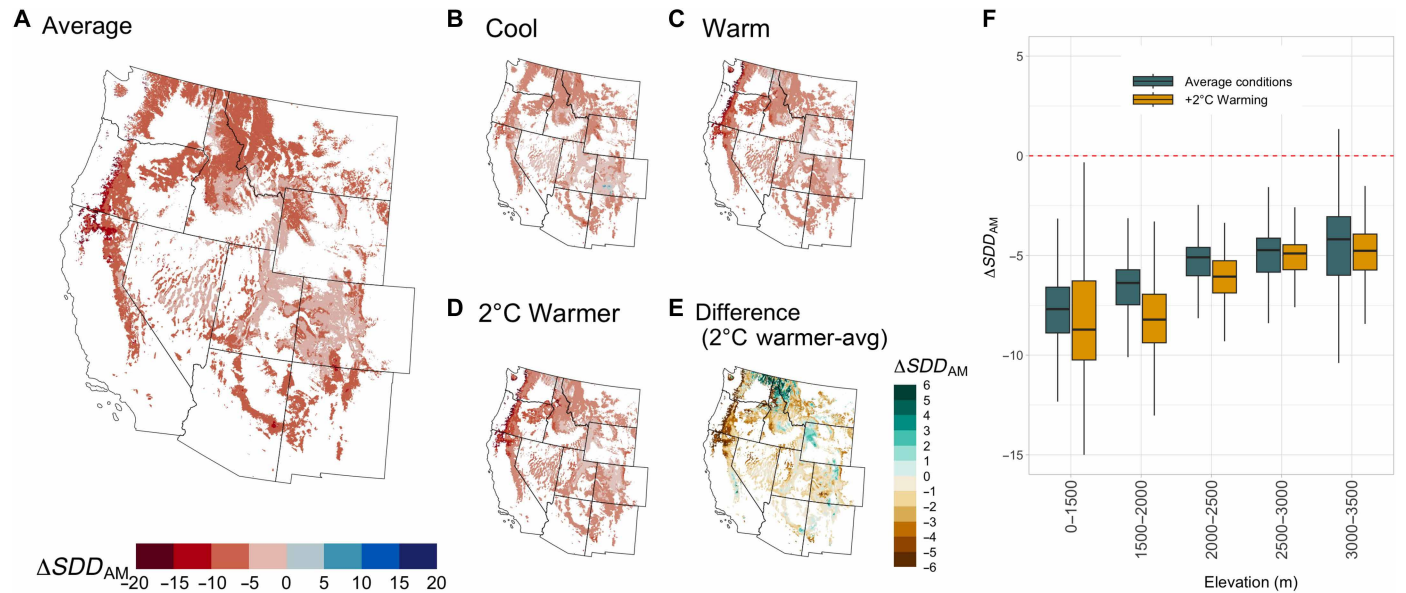


**Fig. 4. Modeled  $\Delta SDD_{AM}$  across the Western US.** Modeled  $\Delta SDD_{AM}$  for the first year following fire under (A) average conditions, (B) cool conditions, (C) warm conditions, (D) +2°C warming relative to average, and (E) the difference between +2°C warming and average conditions. (F) Distribution of  $\Delta SDD_{AM}$  under average conditions and +2°C warming by elevation band.

Downloaded from <https://www.science.org> on October 16, 2025

99% of pixels across the western US melted earlier after a burn compared to predicted unburned conditions with 60% melting out more than 5 days earlier. However, these postfire effects varied regionally and temporally. More pixels in maritime snowpacks [Pacific Northwest (PNW) and Northern California] experienced snow disappearing more than 5 days earlier postfire compared to continental snowpacks in the Intermountain West (Colorado, Utah, Wyoming). At higher elevations in the Intermountain West where conditions are relatively sunny and cold (Fig. 1, C and D), only 34% of pixels showed burned areas melting out more than 5 days earlier than nonburned areas under average climate conditions (Fig. 4A). In contrast, at lower elevations in the PNW, where solar radiation is low and temperatures are warm (Fig. 1, C and D), 95% of pixels melted out more than 5 days earlier postfire under average conditions. In California, although sunnier and warmer than the PNW and with a larger elevation gradient across the Sierra Nevada, 88% of burned pixels melted out more than 5 days earlier than unburned pixels.

We also estimated postfire  $\Delta SDD_{AM}$  for the coldest (Fig. 4B) and warmest (Fig. 4C) winters on record for each pixel. Across the western US, under cold conditions, 98% of pixels experienced snow disappearing later in burned areas compared to nonburned areas, but only 58% experienced more than 5 days later. However, in Colorado, 20% of pixels under cold conditions melted out more than 5 days earlier, compared to 85% of pixels in the PNW (Fig. 4C). In contrast, under warm conditions, the phenomenon of snow disappearing later in burned areas was concentrated in high-elevation, relatively low-solar conditions (Fig. 4C). Under warm conditions, 73% of pixels melted more than 5 days earlier across the western US, while only 53% of pixels in Colorado, Utah, and Wyoming melted more than 5 days earlier in burned areas under warm conditions (Fig. 4C). In Oregon, California, Washington, and Idaho, 90% of pixels had more than a 5 day advance in SDD postfire under warm conditions.

### Fire impacts on SDD under +2°C

We estimated  $\Delta SDD_{AM}$  under a simple warmer climate scenario in which the average winter temperature for each pixel from a historic period of 2002 to 2022 was increased by 2°C to mimic a plausible mid-century mean climate under a wide range of emissions scenarios (46). The precipitation fraction falling as snow was also modified accordingly. In this warmer scenario, the median  $\Delta SDD_{AM}$  advanced an additional 0.9 days on average compared to average conditions across the western US (Fig. 4, D and E), suggesting that the impact of fire on earlier snowmelt could be exacerbated in warmer climate conditions, but impacts would vary regionally. In the +2°C scenario, 71% of the burned pixels had an additional advance in melt timing of 5 days or more relative to average conditions; 75% had had a more negative  $\Delta SDD_{AM}$  than they did in the average scenario.

Impacts of warming on  $\Delta SDD_{AM}$  varied regionally: Oregon experienced the largest shift earlier in  $\Delta SDD_{AM}$  in burned areas, with 2.4 additional days of earlier melt under this warmer climate scenario, followed by California (1.3 days earlier) and Idaho (1.2 days earlier) (Fig. 4E). Washington, Oregon, and California have large negative  $\Delta SDD_{AM}$  under historical average conditions (WA, -7.6 days; OR, -7.7 days; and CA, -6.7 days), and California and Oregon each experienced the largest additional advance in melt in the +2°C scenario. In the Intermountain West,  $\Delta SDD_{AM}$  shifted earlier by more than 5 additional days at 35% of pixels under +2°C of warming compared to historically average conditions (Fig. 4E). Utah, Wyoming,

and Colorado had relatively small  $\Delta SDD_{AM}$  under historical average conditions and had some of the smallest additional advances in  $\Delta SDD_{AM}$  in the +2°C scenario, averaging 0.5 additional days of earlier melt.

### DISCUSSION

Our results indicate that snow predominantly melts earlier after fires, but the magnitude and direction of change in SDD following a fire are strongly influenced by years since burn, elevation, winter temperature, and solar radiation. The persistence of  $\Delta SDD_{LR}$  in the years following a fire is elevation-dependent, with evidence of delayed SDD postfire for 5 to 6 years at middle elevations (2000 to 3000 m) (Fig. 2). The Pacific Northwest and northern Sierra Nevada are most vulnerable to snow disappearing up to 2 weeks earlier after a fire (Fig. 4). Additionally, California and Oregon have the largest additional change in the effect of fire on SDD under +2°C of warming, while the Intermountain West (Colorado, Utah, and Wyoming) experiences small additional earlier melt (Fig. 4). In warmer environments, snow disappearance due to postfire energy balance changes can even occur in midwinter, disrupting the anticipated timing of snowmelt runoff (19).

Most prior literature uses in situ plot scale or distributed SNOTEL observations and emphasizes the importance of increased net shortwave radiation as a driver of postfire SDD changes (21, 23, 37, 40, 41). However, our results indicate that other energy balance components could play larger roles than previously thought. Because low-elevation, warmer snowpacks are persistently near 0°C and are already vulnerable to climate warming, a small change in the snowpack energy balance from decreased albedo (41) can exacerbate the changes in SDD postfire. In contrast, higher-elevation, low-solar, and colder Intermountain West snowpacks are more insulated from fire effects on SDD, with negligible or even positive  $\Delta SDD$  post fire (Fig. 4). Cold, dry snowpacks produce higher cold content that may insulate these areas from severe postfire changes. Therefore, in high-cold-content snowpacks, the increase in net shortwave postfire may not be enough energy to decrease the cold content and initiate markedly earlier melt. As a result, these cold snowpacks have only slightly earlier melt and, in some cases, at the highest elevations, especially in Wyoming, Utah, and Colorado, persist slightly later postfire, potentially due to the increase in snow depth from lack of canopy interception postburn (20, 39, 40, 47).

Elevation, temperature, and incoming solar radiation are strong predictors of changes in SDD postfire and provide important context for why existing literature shows such a large range (4 to 23 days) in SDD advance postfire across the western US (14). This spatial variability is also apparent in how long the effects of fire last; particularly in high-elevation and cold environments, the effects may be relatively small and last for a shorter period than the previously established 10 years (Fig. 3) (20, 40). By five winters after a fire, mid-high elevations (>2000 m) showed a delay in SDD in burned areas (Fig. 2A). At this point, the burned trees still standing may no longer shed black carbon on the snow surface, limiting the reduced albedo effect. These areas may instead experience increased snow accumulation and decreased incoming longwave radiation due to lack of canopy interception. On the basis of our results, we hypothesize that, in the short term, changes in albedo drive postfire SDD, but, in the longer term, SDD is governed by altered canopy structure. Preburn vegetation composition is also highly variable across the western US

and could influence the variability in postfire snowmelt timing. Future studies should consider the interactions between climate conditions and forest composition.

The two statistical methods used in this study complement each other with similar qualitative results but differing quantitative effect sizes. Both illustrate regional spatial variability in postfire SDD across the western US. The effect sizes estimated by the AM were substantially larger than those estimated by the LR. We speculate that this difference could be due to the averaging of LR results across elevation categories and climate conditions after model fitting. The qualitative similarities reinforce confidence in our results, while the quantitative differences imply that structural differences in statistical approaches can affect estimated effect sizes in large-scale statistical studies. Understanding the spatial variability in postfire  $\Delta SDD$  is essential for evaluating where these snowpack changes will affect water resource management and flood forecasting. Because snow contributes a large fraction of streamflow across the western US, earlier SDD can reduce late spring runoff, decreasing streamflow during warmer summer months (48). The loss of snow cover is also a major cause of declining annual flows in large river basins due to enhanced evapotranspiration when snow melts (49). While postfire streamflow can increase water yield in the short term (50) because of decreased evapotranspiration (51, 52), the impacts of fire on snow loss could complicate these changes. Earlier SDD can lead to slower snowmelt when SDD shifts toward a time of year when incoming shortwave radiation is low (53). In relatively warm areas, this shift could decrease snowmelt runoff due to increased deep percolation and subsequent evapotranspiration, while, in colder areas, slower snowmelt could increase runoff (54, 55). The snow regimes with earlier SDD following wildfires (PNW and Northern California) may also be more susceptible to loss of water yield due to earlier SDD (Fig. 4). All these factors contribute to a disruption in the quantity and timing of water availability derived from snowmelt, especially in the PNW and Northern California.

Anthropogenic climate change is projected to cause warmer winter temperatures across the western US (56). These increased winter temperatures could further advance SDD in burned areas. In the future, the effects of fire could be more widespread than under historically average conditions and continue to exacerbate effects in already vulnerable areas like Oregon. Additionally, the areas that experience minimal postfire advance of SDD under historical conditions may experience the largest change in postfire SDD advance in warmer conditions like the Intermountain West (Fig. 4). Our results suggest that the impact of wildfires on snow cover loss could increase in warmer climates, which could further strain snow-derived water resources in the future. Postfire changes should be incorporated into land surface, flood, and streamflow forecasting models, particularly in the most vulnerable regions. Fire is also projected to advance to higher elevations (15), where our results indicate snowpacks are less vulnerable to snow cover loss. However, it is unclear whether this upslope advance would decrease the effects of fire on snow or whether these high-elevation environments would look increasingly like lower-elevation environments of recent decades. In the near term, as wildfires continue to burn higher into the snow zone across much of the western US (20, 21), a more nuanced understanding of conditions that exacerbate the impacts of fires on snow cover loss helps focus our efforts of concern for water management in burned watersheds.

## MATERIALS AND METHODS

### Datasets

#### Snow disappearance date

SDD is calculated from STC-MODSCAG, a daily fractional snow cover product derived from MODIS surface reflectance bands that produces a STC dataset at nominal 500-m resolution (463 m) (Fig. 1A) (44). Using multiple-end member spectral mixture analysis, MODSCAG solves for subpixel fractional snow-covered area (fSCA) and grain size of the fractional snow cover. MODSCAG allows the snow spectral reflectance to vary by pixel to account for the spatial heterogeneity of snow in mountainous terrain. MODSCAG is known to underestimate viewable snow under the canopy, resulting in underestimates of on the ground snow in dense canopy (45). However, with recent improvements and compared to other remote sensing products, STC-MODSCAG performs well in mountain forests, especially when canopy cover is less than 70% (45, 57). Specifically, STC-MODSCAG has an RMSE of 0.119 m relative to Airborne Snow Observatory (ASO) fSCA, where ASO fSCA is calculated from lidar-derived 3-m snow depth converted to a binary snow-cover map with a threshold of 8 cm to define snow-free pixels. Therefore, STC-MODSCAG provides a more accurate snow-covered area, especially in forested areas, than the standard MOD10A1 product that is a binary product of “snow” or “no snow” classified by the normalized difference snow index (57, 58).

We calculated SDD for each WY by identifying the first date at which each pixel switches from snow (greater than 15% snow cover) to no snow (less than 15% snow cover) following Crumley *et al.* (59). We required at least 10 days of snow cover preceding the calculated SDD to ensure that ephemeral late-season snow events were not captured. We also set a threshold of nonconsecutive 30 days of snow cover per WY to count as a snowy pixel to avoid ephemeral snowpacks. We masked out pixels with greater than 70% canopy cover as determined by the National Land Cover Dataset (NLCD) because STC-MODSCAG is validated to perform well under tree canopy up to 70% tree cover (45, 57, 60). This resulted in a removal of 0.018% of pixels in the snow zone (fig. S1). Because we are most interested in forests where a fire could burn, pixels were filtered to land covers of evergreen forest, shrub lands, deciduous forest, and mixed forest as labeled in the NLCD. SDD was calculated for each pixel in the seasonal snow zone across the western US for each WY over the 20 years of available data (WYs 2002 to 2022).

#### Fire data

Burned pixels are identified using the Monitoring Trends in Burn Severity (MTBS), an interagency dataset produced by the United States Geological Survey, United States Forest Service, and United States Department of Agriculture with the goal of producing a long-term dataset of burn severity and extent of large fires across the US since 1984 (fig. S2). This dataset includes fires greater than 1000 acres in the western US and greater than 500 acres in the eastern US. Fire data are derived from NASA Landsat at 30-m resolution by calculating the difference in the normalized burn ratio (dNBR) using a normalized band ratio of Near Infrared (NIR) to Shortwave-Infrared (SWIR) (61). This is the most comprehensive fire dataset for the entire US, providing data from 1984 to 2021 that include all burn severities. We filtered each burn severity raster to only include pixels labeled as low, moderate, or high burn severity and resampled the rasters to the nominal 500-m resolution of STC-MODSCAG by identifying pixels as “burned” if more than 50% of the 30-m pixels

were burned in each 500-m pixel. We only used data from 2000 to 2021, constrained by the overlap of our masked STC-MODSCAG and MTBS datasets (fig. S2).

### Climate variables

Estimated annual snowfall, average winter temperatures (December to April), and average winter incoming solar radiation (December to April) were derived from gridMET, a daily 4-km reanalysis surface meteorological dataset. gridMET is a climatically aided interpolation of gridded climate data developed using PRISM with temporal features from NLDAS-2, validated against an extensive network of weather stations (Fig. 1, C to E, and fig. S3) (43). Using the nearest neighbor method, we assigned gridMET values to STC-MODSCAG pixels. Estimated annual liquid snowfall equivalent (*SFE*) was calculated by summing pixelwise daily precipitation that occurred when the daily average temperature was below 1°C (62). Sensitivity tests indicated that our qualitative results were unaffected by the precipitation phase threshold (fig. S4). Average winter temperatures ( $T_{\text{avg}}$ ) were calculated by averaging daily minimum and maximum temperatures from December to April and then taking an average of those values for each winter. For the future climate scenario, 2°C was added to average winter temperatures, and annual *SFE* was recalculated using +2°C temperatures, retaining the 1°C precipitation phase threshold.

The gridMET solar radiation accounts for cloud cover effects but is estimated on a flat surface. We terrain corrected the gridMET radiation using the “insol” package (63) in the R programming language. The algorithm accounts for aspect, self-shading, slope, and shading by adjacent terrain. We calculated a terrain correction factor by dividing the terrain-calculated solar radiation by the flat digital elevation model (DEM) where all elevation values were equal to the mean elevation of the nominal 500-m DEM (64). Where terrain enhances solar radiation (e.g., south-facing slopes), the correction factor is greater than 1, and where the terrain diminishes the solar radiation (e.g., shaded valleys), the correction factor is less than 1. We then calculated average winter solar radiation values across the western US by running the algorithm at a daily time step from December to April using fixed parameter values for visibility (30 km), relative humidity (50%), and temperature (273 K). These parameter values are realistic for winter in the seasonal snow zone of the western US, and the relative values comprising the terrain correction factor are insensitive to parameter values (64). We multiplied the gridMET solar radiation by the terrain correction factor to derive the average winter terrain-corrected solar radiation for each year of the study (Fig. 1D). All gridMET variables were resampled using the nearest neighbor method to downscale from 4 km to the native resolution of STC-MODSCAG (Fig. 1D and fig. S3).

We also calculated the annual number of days with snowfall by summing the number of days per WY that received more than 1 mm of precipitation when the average temperature was less than 1°C (35). A snowfall intensity factor was calculated by dividing the total amount of estimated snowfall by the number of wet days (65). Neither of these metrics was used in the final selected additive model because they did not enhance the cross-validated fit statistics of the model.

### Forest classification

We used an established climate-forest-snow classification that classifies pixels by melt patterns and winter temperatures (47). This classification is based on a decision tree that ranks forest-snow interaction variables that influence snow storage (duration and magnitude) in the forest including wind, winter ambient temperatures,

and magnitude of forest shading at 800-m resolution (fig. S5) (47). This spatial classification was downscaled to the native resolution of STC-MODSCAG using the nearest neighbor method.

### Statistical analysis

We used two different statistical approaches to complement each other in assessing the impacts of burned forests on SDD across the western US

#### Pixelwise LR

To estimate the pixelwise effect of fire on SDD, we fit LRs of *SDD* as a function of *SFE* and winter  $T_{\text{avg}}$  over the period before burn. For each pixel  $i$ , a model was estimated for preburn WY  $j$

$$SDD_{ij} = \beta + \beta_1(T_{\text{avg}_{ij}}) + \beta_2(SFE_{ij}) \quad (1)$$

$$\epsilon \sim N(0, \Delta\sigma^2) \quad (2)$$

where  $T_{\text{avg}}$  is the average winter temperature from December to April and *SFE* is the annual estimated snowfall for each WY per pixel. Errors are normally distributed (Eq. 2), with some evidence of long tails (fig. S6). For this model fitting, the data were filtered to only pixels that had at least 17 years of data to ensure a long enough record for accurate fit and postfire data on which to assess the burn effect.

The LR was estimated for each pixel that burned between 2010 and 2021, using this relatively late burn period to ensure that pixels had enough preburn data to fit a regression. For each pixel, the LR was fit on the WYs before the burn and predicted over the entire time series for each pixel, including postfire years. For each postfire year, we calculated the difference between the postfire observed SDD and predicted SDD by the regression model.

Each burned pixel was matched with a nearby pixel that did not burn between 2000 and 2021 as classified by the MTBS dataset. Matches were determined by identifying pixels within the same 500-m elevation band, NLCD-based land cover, and aspect and then selecting a match to minimize Euclidean distance in  $x$ - $y$  space using an Albers equal area projection. The LR was applied to the matching unburned pixels in the same manner as for the burned pixel, and the prediction error in the postfire period was similarly calculated (fig. S7). We estimated the fire effect size ( $\Delta SDD_{\text{LR}}$ ) by subtracting the residual (predicted SDD – observed SDD) of each unburned matching pixel from the residual of the burned pixel. This approach controls for unobserved climate variation that might systematically bias the estimate of  $\Delta SDD_{\text{LR}}$  if it was calculated on the basis of the burned pixel prediction errors alone. The same calculation was conducted over the prefire period to ensure that no apparent burn effect existed prefire. This statistical analysis was performed on more than 91,000 burned pixels across the western US. The average  $R^2$  value across burned pixels was 0.46, and average  $R^2$  value for unburned pixels was 0.47.

To assess the statistical significance of  $\Delta SDD_{\text{LR}}$ , we calculated the mean and 95% CI of  $\Delta SDD_{\text{LR}}$  for each elevation bin and year since burn.  $\Delta SDD_{\text{LR}}$  values were considered significant when the CI bounds did not include zero. Parametric CIs were calculated by extracting the 2.5th and 97.5th quantiles from the normal distribution and multiplying the *SE* by the resulting value; the resulting values were added to and subtracted from the mean to construct the CI. An important issue is that the observations were spatially autocorrelated, reducing the effective sample size (66). Therefore, we calculated

Moran's  $I$  using the “spdep” R package (67), which characterizes the degree of spatial autocorrelation, for each year since burn and 500-m elevation band. Following Dale and Fortin (68), the effective sample size was then calculated as

$$N_{\text{eff}} = N \frac{1 - I}{1 + I} \quad (3)$$

where  $N$  is the sample size and  $N_{\text{eff}}$  is the effective sample size (68).  $N_{\text{eff}}$  was then applied in the calculations of the SE to remove the effect of spatial autocorrelation in the CI calculations.

#### Additive model

To complement the linear model approach and develop a statistical model of fire impacts on SDD that could be applied across the western US, we fit an additive model (69) that accounts for spatial variability to determine which variables have the largest influence on SDD in postfire environments. Similar model structures have been previously applied to snow hydrology (65, 70). All burned pixels in the dataset were selected, while an equal number of unburned pixels were sampled to match. Using the “mgcv” package in the R programming language (71), we fit an additive model to the sampled data. This method was chosen to account for temporal and spatial correlation structures in the dataset and allow for nonlinear effects and interactions. The model for SDD in WY  $j$  at each pixel  $i$  was constructed as

$$SDD_{ij} = \alpha + f_1(\text{srad}_{ij}, T_{\text{avg}_{ij}}, \text{burn}_i) + f_2(\text{SFE}_{ij}, \text{elev}_i, \text{snowtype}_i) + f_3(\text{year since}_{ij}) + f_4(x, y) + \epsilon_{ij} \quad (4)$$

$$\epsilon \sim N(0, \Delta\sigma^2) \quad (5)$$

where SDD is the snow disappearance date,  $\alpha$  is the intercept,  $f_1$  and  $f_2$  are tensor product interactions of thin-plate splines, and  $f_3$  and  $f_4$  are thin-plate splines. The model includes elevation (*elev*), average winter solar radiation from December to April (*srad*), average winter temperature from December to April ( $T_{\text{avg}}$ ), annual estimated snowfall (*SFE*), whether a pixel burned (*burn*), snow type based on forest/snow classification (*snow type*) (47), years since burn (*year since*), latitude ( $y$ ), and longitude ( $x$ ). All errors are approximately normally distributed (fig. S8). The basis dimension used to represent the smoothed terms,  $k$ , was set to 6 for  $f_1$  and  $f_2$  and 100 for  $f_4$  to minimize cross-validated RMSE. Although *srad* and  $y$  are highly correlated (fig. S9) and initial assessment of the model indicated high concurrency, the inclusion of spatial terms in the model alleviated spatial patterns in the residuals (fig. S8) (71). Aspect was not included in the model because the impact of aspect is captured in the terrain-corrected *srad*.

Spatial residuals were inspected for heteroskedasticity and normality and to ensure that no spatial patterns were present (fig. S8). A 10-fold cross-validation was performed to ensure predictability of the model and avoid overfitting (72). The specific model structure was selected to minimize the cross-validated RMSE. Residuals show a lack of spatial patterns and an approximately normal distribution, with some outlying observations (fig. S8). The model is also designed to minimize concurrency by removing redundant variables. We tested multiple possible distributions of the response variable, and ultimately proceeded with the Gaussian distribution for best normality of the residuals and minimal cross-validated RMSE. The model cross-validated RMSE was 14.87 days, with an  $R^2$  value of 0.74. Cross-

validated RMSE was 0.13 days higher than training data RMSE. Final model metrics were assessed on the average of the cross-validation of the out-of-sample 10% of data after the 10-fold analysis (72).

To estimate  $\Delta SDD$  with the additive model ( $\Delta SDD_{\text{AM}}$ ), we use the additive model to predict SDD in hypothetical burned and unburned conditions across a matrix of temperature and solar radiation values (Fig. 3, B and C) and subtract the two resulting rasters to illustrate the  $\Delta SDD_{\text{AM}}$  in the temperature-solar radiation variable space (Fig. 3D). To assess spatial variability in  $\Delta SDD_{\text{AM}}$  across the Western US, we predict SDD under hypothetical burned and unburned conditions for each pixel using its average climate conditions. To assess  $\Delta SDD_{\text{AM}}$  in relatively cool and warm conditions, we identified the coldest and warmest winter temperatures on record for each pixel from WYs 2002 to 2022 and calculated  $\Delta SDD_{\text{AM}}$  as in the historical average case, keeping all other variables consistent.

The warmer climate scenario was estimated by adding 2°C to the mean winter temperature from 2002 to 2022. This method was chosen to mimic mid-century climate warming within the uncertainty bounds of scenarios ranging from relatively low- to high-emission cases (46). We then calculated the  $\Delta SDD_{\text{AM}}$  for this warmer climate scenario as calculated in the historical scenario. The difference between  $\Delta SDD_{\text{AM}}$  in the +2°C scenario versus the historical average is obtained by subtracting the two rasters of estimated  $\Delta SDD_{\text{AM}}$ . All statistical and graphical analysis was performed in the R programming language version 4.4.1. (73).

#### Assumptions and limitations

Satellite remote sensing remains somewhat limited in its ability to detect fSCA in densely covered forests. To help minimize this problem, we used the STC-MODSCAG reanalysis product that performs well under tree canopy up to 70% tree cover (45, 57, 60). The nominal 500-m scale does not capture microclimates or small-scale terrain influence on snow accumulation and melt patterns. We only assess snow-cover fraction from satellite imagery, so this approach is limited to only assessing SDD, not snow water equivalent or melt rates. Despite these caveats, analysis with remote sensing data has strengths that complement the limitations associated with site-scale studies or SNOTEL analysis in understanding large-scale changes across the western US. Here, we use the best data available to assess spatial and temporal variability in wildfire impacts on snow hydrology across the Western US.

There is some quantitative disagreement between the LR and additive model providing uncertainty in the change in SDD post fire, but the alignment of spatial pattern and effect direction provides confidence in overall conclusions, while the inclusion of both statistical approaches exposes uncertainty from statistical model structure. The LR model is limited to only pixels that burned in 2010 or later. The unburned matched pixels could also have soot or debris transported by wind from the burned pixel onto the snowpack, potentially explaining the smaller effect size in the LR. The LR is constructed of three parameters using a sample size of 9 to 19 data points per pixel. Although the relatively few degrees of freedom can yield model uncertainty, the spatial and temporal coherence of results and directional consistency with the additive model provide added confidence in our results. The additive model allows us to predict the effect of fire over pixels that have never burned but has a slightly less flexible representation of the fire impact. These approaches, therefore, have complementary limitations and advantages in helping understand the spatial and temporal variability in wildfire impacts on snow hydrology.

Last, future climate projections encompass more than just temperature changes. Most notably, specific humidity, solar intensity at the surface, and precipitation intensity are all projected to change under future climate projections. While this study does not explicitly address these factors, they could substantially influence how wildfire affects snow disappearance in a changing climate given their roles in governing patterns of snowpack dynamics.

## Supplementary Materials

### This PDF file includes:

Figs. S1 to S9

Table S1

## REFERENCES AND NOTES

- D. Viviroli, H. H. Dürr, B. Messerli, M. Meybeck, R. Weingartner, Mountains of the world, water towers for humanity: Typology, mapping, and global significance. *Water Resour. Res.* **43**, W07447 (2007).
- P. R. Kormos, C. H. Luce, S. J. Wenger, W. R. Berghuijs, Trends and sensitivities of low streamflow extremes to discharge timing and magnitude in Pacific Northwest mountain streams. *Water Resour. Res.* **52**, 4990–5007 (2016).
- A. M. Marshall, J. M. Chen, Impacts of changing snowfall on seasonal complementarity of hydroelectric and solar power. *Environ. Res. Infrastruct. Sustain.* **2**, 021001 (2022).
- H. Yan, N. Sun, A. Fullerton, M. Baerwalde, Greater vulnerability of snowmelt-fed river thermal regimes to a warming climate. *Environ. Res. Lett.* **16**, 054006 (2021).
- D. Li, M. L. Wrzesien, M. Durand, J. Adam, D. P. Lettenmaier, How much runoff originates as snow in the Western United States, and how will that change in the future? *Geophys. Res. Lett.* **44**, 6163–6172 (2017).
- A. M. Marshall, J. T. Abatzoglou, T. E. Link, C. J. Tennant, Projected changes in interannual variability of peak snowpack amount and timing in the Western United States. *Geophys. Res. Lett.* **46**, 8882–8892 (2019).
- E. R. Siirila-Woodburn, A. M. Rhoades, B. J. Hatchett, L. S. Huning, J. Szinaï, C. Tague, P. S. Nico, D. R. Feldman, A. D. Jones, W. D. Collins, L. Kaatz, A low-to-no snow future and its impacts on water resources in the Western United States. *Nat. Rev. Earth Environ.* **2**, 800–819 (2021).
- A. Harpold, P. D. Brooks, S. Rajagopal, I. Heidbuchel, A. Jardine, C. Stielstra, Changes in snowpack accumulation and ablation in the intermountain west. *Water Resour. Res.* **48**, 1–11 (2012).
- D. S. O'Leary III, D. K. Hall, N. E. DiGirolamo, G. A. Riggs, Regional trends in snowmelt timing for the western United States throughout the MODIS era. *Phys. Geogr.* **43**, 285–307 (2022).
- C. W. Thackeray, C. G. Fletcher, L. R. Mudryk, C. Derksen, Quantifying the uncertainty in historical and future simulations of Northern Hemisphere spring snow cover. *J. Clim.* **29**, 8647–8663 (2016).
- R. Essery, H. Kim, L. Wang, P. Bartlett, A. Boone, C. Brutel-Vuilmet, E. Burke, M. Cuntz, B. Decharme, E. Dutra, X. Fang, Y. Gusev, S. Hagemann, V. Haverd, A. Kontu, G. Krinner, M. Lafaysse, Y. Lejeune, T. Marke, D. Marks, C. Marty, C. B. Menard, O. Nasonova, T. Nitta, J. Pomeroy, G. Schädler, V. Semenov, T. Smirnova, S. Swenson, D. Turkov, N. Wever, H. Yuan, Snow cover duration trends observed at sites and predicted by multiple models. *Cryosphere* **14**, 4687–4698 (2020).
- L. Mudryk, M. Santolaria-Otín, G. Krinner, M. Ménégou, C. Derksen, C. Brutel-Vuilmet, M. Brady, R. Essery, Historical Northern Hemisphere snow cover trends and projected changes in the CMIP6 multi-model ensemble. *Cryosphere* **14**, 2495–2514 (2020).
- J. T. Overpeck, B. Udall, Climate change and the aridification of North America. *Proc. Natl. Acad. Sci. U.S.A.* **117**, 11856–11858 (2020).
- A. L. Koshkin, B. J. Hatchett, A. W. Nolin, Wildfire impacts on western United States snowpacks. *Front. Water* **4**, 971271 (2022).
- M. R. Alizadeh, J. T. Abatzoglou, C. H. Luce, J. F. Adamowski, A. Farid, M. Sadegh, Warming enabled upslope advance in western US forest fires. *Proc. Natl. Acad. Sci. U.S.A.* **118**, e2009717118 (2021).
- S. A. Parks, J. T. Abatzoglou, Warmer and drier fire seasons contribute to increases in area burned at high severity in Western US forests from 1985 to 2017. *Geophys. Res. Lett.* **47**, e2020GL089858 (2020).
- Z. A. Holden, A. Swanson, C. H. Luce, W. M. Jolly, M. Maneta, J. W. Oyler, D. A. Warren, R. Parsons, D. Affleck, Decreasing fire season precipitation increased recent western US forest wildfire activity. *Proc. Natl. Acad. Sci. U.S.A.* **115**, E8349–E8357 (2018).
- A. L. Westerling, H. G. Hidalgo, D. R. Cayan, T. W. Swetnam, Warming and earlier spring increase western U.S. forest wildfire activity. *Science* **313**, 940–943 (2006).
- B. J. Hatchett, A. L. Koshkin, K. Guirguis, K. Rittger, A. W. Nolin, A. Heggli, A. M. Rhoades, A. E. East, E. R. Siirila-Woodburn, W. T. Brandt, A. Gershunov, K. Haleakala, Midwinter dry spells amplify post-fire snowpack decline. *Geophys. Res. Lett.* **50**, e2022GL101235 (2023).
- K. E. Gleason, J. R. McConnell, M. M. Arienzo, N. Chellman, W. M. Calvin, Four-fold increase in solar forcing on snow in western U.S. burned forests since 1999. *Nat. Commun.* **10**, 2026 (2019).
- S. K. Kampf, D. McGrath, M. G. Sears, S. R. Fassnacht, L. Kiewiet, J. C. Hammond, Increasing wildfire impacts on snowpack in the western U.S. *Proc. Natl. Acad. Sci. U.S.A.* **119**, e2200333119 (2022).
- J. Dozier, S. R. Schneider, D. F. McGinnis, Effect of grain size and snowpack water equivalence on visible and near-infrared satellite observations of snow. *Water Resour. Res.* **17**, 1213–1221 (1981).
- K. E. Gleason, A. W. Nolin, T. R. Roth, Charred forests increase snowmelt: Effects of burned woody debris and incoming solar radiation on snow ablation. *Geophys. Res. Lett.* **40**, 4654–4661 (2013).
- N. P. Molotch, M. T. Colee, R. C. Bales, J. Dozier, Estimating the spatial distribution of snow water equivalent in an alpine basin using binary regression tree models: The impact of digital elevation data and independent variable selection. *Hydrol. Process.* **19**, 1459–1479 (2005).
- W. J. Wiscombe, S. G. Warren, A model for the spectral albedo of snow. *J. Atmos. Sci.* **37**, 2712–2733 (1980).
- A. Varhola, N. C. Coops, M. Weiler, R. D. Moore, Forest canopy effects on snow accumulation and ablation: An integrative review of empirical results. *J. Hydrol.* **392**, 219–233 (2010).
- K. Burles, S. Boon, Snowmelt energy balance in a burned forest plot, Crowsnest Pass, Alberta, Canada. *Hydrol. Process* **25**, 3012–3029 (2011).
- A. A. Harpold, J. A. Biederman, K. Condon, M. Merino, Y. Korgaonkar, T. Nan, L. L. Sloat, M. Ross, P. D. Brooks, Changes in snow accumulation and ablation following the Las Conchas Forest Fire, New Mexico, USA. *Ecology* **7**, 440–452 (2014).
- J. D. Lundquist, S. E. Dickerson-Lange, J. A. Lutz, N. C. Cristea, Lower forest density enhances snow retention in regions with warmer winters: A global framework developed from plot-scale observations and modeling: Forests and Snow Retention. *Water Resour. Res.* **49**, 6356–6370 (2013).
- T. R. Roth, A. W. Nolin, Forest impacts on snow accumulation and ablation across an elevation gradient in a temperate montane environment. *Hydrol. Earth Syst. Sci.* **21**, 5427–5442 (2017).
- C. R. Ellis, J. W. Pomeroy, R. L. H. Essery, T. E. Link, Effects of needleleaf forest cover on radiation and snowmelt dynamics in the Canadian Rocky Mountains. *Can. J. For. Res.* **41**, 608–620 (2011).
- D. A. Faria, J. W. Pomeroy, R. L. H. Essery, Effect of covariance between ablation and snow water equivalent on depletion of snow-covered area in a forest. *Hydrol. Process.* **14**, 2683–2695 (2000).
- S. Boon, Snow ablation energy balance in a dead forest stand. *Hydrol. Process.* **23**, 2600–2610 (2009).
- A. N. Gelfan, J. W. Pomeroy, L. S. Kuchment, Modeling forest cover influences on snow accumulation, sublimation, and melt. *J. Hydrometeorol.* **5**, 785–803 (2004).
- K. S. Jennings, N. P. Molotch, Snowfall fraction, cold content, and energy balance changes drive differential response to simulated warming in an alpine and subalpine snowpack. *Front. Earth Sci.* **8**, 186 (2020).
- P. Marsh, Grain growth in a wet arctic snow cover. *Cold Reg. Sci. Technol.* **14**, 23–31 (1987).
- D. McGrath, L. Zeller, R. Bonnell, W. Reis, S. Kampf, K. Williams, M. Okal, A. Olsen-Mikitowicz, E. Bump, M. Sears, K. Rittger, Declines in peak snow water equivalent and elevated snowmelt rates following the 2020 Cameron peak wildfire in Northern Colorado. *Geophys. Res. Lett.* **50**, e2022GL101294 (2023).
- P. D. Micheletty, A. M. Kinoshita, T. S. Hogue, Application of MODIS snow cover products: Wildfire impacts on snow and melt in the Sierra Nevada. *Hydrol. Earth Syst. Sci.* **18**, 4601–4615 (2014).
- T. M. Uecker, S. D. Kaspari, K. N. Musselman, S. McKenzie Skiles, The post-wildfire impact of burn severity and age on black carbon snow deposition and implications for snow water resources, cascade range, Washington. *J. Hydrometeorol.* **21**, 1777–1792 (2020).
- J. Giovando, J. D. Niemann, Wildfire impacts on snowpack phenology in a changing climate within the Western U.S. *Water Resour. Res.* **58**, e2021WR031569 (2022).
- E. E. Smoot, K. E. Gleason, Forest fires reduce snow-water storage and advance the timing of snowmelt across the Western U.S. *Water* **13**, 3533 (2021).
- J. N. Herbert, M. S. Raleigh, E. E. Small, Reanalyzing the spatial representativeness of snow depth at automated monitoring stations using airborne lidar data. *Cryosphere* **18**, 3495–3512 (2024).
- J. T. Abatzoglou, Development of gridded surface meteorological data for ecological applications and modelling. *Int. J. Climatol.* **33**, 121–131 (2013).
- K. Rittger, S. J. Lenard, R. T. Palomaki, M. J. Brodzik, T. Stilling, E. H. Bair, J. Dozier, T. H. Painter, “Historical MODIS/Terra L3 Global Daily 500m SIN Grid Snow Cover, Snow Albedo, and Snow Physical Properties, Version 1,” National Snow and Ice Data Center (2025); [https://nsidc.org/data/stc\\_modsgrd\\_hist/versions/1](https://nsidc.org/data/stc_modsgrd_hist/versions/1).
- K. Rittger, M. S. Raleigh, J. Dozier, A. F. Hill, J. A. Lutz, T. H. Painter, Canopy adjustment and improved cloud detection for remotely sensed snow cover mapping. *Water Resour. Res.* **56**, e2019WR024914 (2020).

46. "Cross-Section Box TS.1, Figure 1," IPCC (2021); [www.ipcc.ch/report/ar6/wg1/figures/technical-summary/ts-cbox-1-figure-1/](http://www.ipcc.ch/report/ar6/wg1/figures/technical-summary/ts-cbox-1-figure-1/).
47. S. E. Dickerson-Lange, J. A. Vano, R. Gersonde, J. D. Lundquist, Ranking forest effects on snow storage: A decision tool for forest management. *Water Resour. Res.* **57**, e2020WR027926 (2021).
48. J. C. Hammond, F. A. Saavedra, S. K. Kampf, How does snow persistence relate to annual streamflow in mountain watersheds of the Western U.S. with wet maritime and dry continental climates? *Water Resour. Res.* **54**, 2605–2623 (2018).
49. P. C. D. Milly, K. A. Dunne, Colorado River flow dwindles as warming-driven loss of reflective snow energizes evaporation. *Science* **367**, 1252–1255 (2020).
50. A. P. Williams, B. Livneh, K. A. McKinnon, W. D. Hansen, J. S. Mankin, B. I. Cook, J. E. Smerdon, A. M. Varuolo-Clarke, N. R. Bjarke, C. S. Juang, D. P. Lettenmaier, Growing impact of wildfire on western US water supply. *Proc. Natl. Acad. Sci. U.S.A.* **119**, e2114069119 (2022).
51. D. W. Hallema, G. Sun, P. V. Caldwell, S. P. Norman, E. C. Cohen, Y. Liu, K. D. Bladon, S. G. McNulty, Burned forests impact water supplies. *Nat. Commun.* **9**, 1307 (2018).
52. M. L. Wine, D. Cadol, O. Makhnin, In ecoregions across western USA streamflow increases during post-wildfire recovery. *Environ. Res. Lett.* **13**, 014010 (2018).
53. K. N. Musselman, M. P. Clark, C. Liu, K. Ikeda, R. Rasmussen, Slower snowmelt in a warmer world. *Nat. Clim. Change* **7**, 214–219 (2017).
54. T. B. Barnhart, C. L. Tague, N. P. Molotch, The counteracting effects of snowmelt rate and timing on runoff. *Water Resour. Res.* **56**, e2019WR026634 (2020).
55. E. Trujillo, N. P. Molotch, Snowpack regimes of the Western United States. *Water Resour. Res.* **50**, 5611–5623 (2014).
56. IPCC, *Global Warming of 1.5°C: IPCC Special Report on Impacts of Global Warming of 1.5°C above Pre-Industrial Levels in Context of Strengthening Response to Climate Change, Sustainable Development, and Efforts to Eradicate Poverty* (Cambridge Univ. Press, ed. 1, 2022); [www.cambridge.org/core/product/identifier/9781009157940/type/book](http://www.cambridge.org/core/product/identifier/9781009157940/type/book).
57. T. Stillinger, K. Rittger, M. S. Raleigh, A. Mitchell, R. E. Davis, E. H. Bair, Landsat, MODIS, and VIIRS snow cover mapping algorithm performance as validated by airborne lidar datasets. *Cryosphere* **17**, 567–590 (2023).
58. T. H. Painter, K. Rittger, C. McKenzie, P. Slaughter, R. E. Davis, J. Dozier, Retrieval of subpixel snow covered area, grain size, and albedo from MODIS. *Remote Sens. Environ.* **113**, 868–879 (2009).
59. R. L. Crumley, R. T. Palomaki, A. W. Nolin, E. A. Sproles, E. J. Mar, SnowCloudMetrics: Snow information for everyone. *Remote Sens* **12**, 3341 (2020).
60. M. S. Raleigh, K. Rittger, C. E. Moore, B. Henn, J. A. Lutz, J. D. Lundquist, Ground-based testing of MODIS fractional snow cover in subalpine meadows and forests of the Sierra Nevada. *Remote Sens. Environ.* **128**, 44–57 (2013).
61. J. Eidsenink, B. Schwind, K. Brewer, Z.-L. Zhu, B. Quayle, S. Howard, A project for monitoring trends in burn severity. *Fire Ecol.* **3**, 3–21 (2007).
62. K. S. Jennings, T. S. Winchell, B. Livneh, N. P. Molotch, Spatial variation of the rain–snow temperature threshold across the Northern Hemisphere. *Nat. Commun.* **9**, 1148 (2018).
63. J. Corripio, "insol" package, version 1.1.1, meteoexploration (2014); [www.meteoexploration.com/R/insol/index.html](http://www.meteoexploration.com/R/insol/index.html).
64. A. C. Lute, J. T. Abatzoglou, Best practices for estimating near-surface air temperature lapse rates. *Int. J. Climatol.* **41**, E110–E125 (2021).
65. A. M. Marshall, T. E. Link, A. P. Robinson, J. T. Abatzoglou, Higher snowfall intensity is associated with reduced impacts of warming upon winter snow ablation. *Geophys. Res. Lett.* **47**, e2019GL086409 (2020).
66. R. S. Bivand, E. Pebesma, V. Gómez-Rubio, *Applied Spatial Data Analysis with R* (Springer, 2013); <https://link.springer.com/10.1007/978-1-4614-7618-4>.
67. R. Bivand, R packages for analyzing spatial data: A comparative case study with areal data. *Geogr. Anal.* **54**, 488–518 (2022).
68. M. R. T. Dale, M.-J. Fortin, *Spatial Analysis: A Guide For Ecologists* (Cambridge Univ. Press, Cambridge, ed. 1, 2005).
69. S. N. Wood, *Generalized Additive Models: An Introduction with R, Second Edition* (Chapman and Hall/CRC, ed. 2, 2017).
70. E. L. Montoya, J. Dozier, W. Meiring, Biases of April 1 snow water equivalent records in the Sierra Nevada and their associations with large-scale climate indices. *Geophys. Res. Lett.* **41**, 5912–5918 (2014).
71. S. N. Wood, Fast stable restricted maximum likelihood and marginal likelihood estimation of semiparametric generalized linear models. *J. R. Stat. Soc. Series B Stat. Methodol.* **73**, 3–36 (2011).
72. D. Berrar, "Cross-Validation," in *Encyclopedia of Bioinformatics and Computational Biology*, S. Ranganathan, M. Gribskov, K. Nakai, C. Schönbach, Eds. (Academic Press, 2019), pp. 542–545; [www.sciencedirect.com/science/article/pii/B978012809633820349X](http://www.sciencedirect.com/science/article/pii/B978012809633820349X).
73. R Core Team, R: A Language and Environment for Statistical Computing, R Foundation for Statistical Computing (2024); [www.R-project.org/](http://www.R-project.org/).

**Acknowledgments:** We would like to thank the reviewers for comments that substantially improved the manuscript. Comments from R. Venturini and D. Nychka improved the presentation and statistical methods of the manuscript. **Funding:** A.K. and A.M. were supported by Dr. Marshall's start-up funding at the Colorado School of Mines. K.R. was supported by NASA grants 80NSSC22K0929, 80NSSC22K0703, 80NSSC23K0793, and 80NSSC22K0686. **Author contributions:** Conceptualization: A.K. and A.M. Methodology: A.K. and A.M. Investigation: A.K. Visualization: A.K. Writing—original draft: A.K. Writing—review and editing: A.K., A.M., and K.R. Funding acquisition: A.M. Data curation: A.M., K.R., and A.K. Formal analysis: A.K. and K.R. Validation: A.K. and K.R. Resource: K.R. Software: K.R. and A.K. Supervision: A.M. Project administration: A.M. **Competing interests:** The authors declare that they have no competing interests. **Data and materials availability:** All data needed to evaluate the conclusions in the paper are present in the paper and/or the Supplementary Materials. The data used in this work came from gridMET ([www.northwestknowledge.net/metdata/data/](http://www.northwestknowledge.net/metdata/data/)), the Monitoring Trends in Burn Severity (MTBS; <http://mtbs.gov/direct-download>), STC-MODSCAG (<https://doi.org/10.7265/f6j3-f387>), Snow Disappearance Date (SDD; <https://doi.org/10.5281/zenodo.13386754>), and forest type ([www.hydroshare.org/resource/76e60d8b9ead4c33898c14dd677c6e06/](http://www.hydroshare.org/resource/76e60d8b9ead4c33898c14dd677c6e06/)). Code used to generate the figures and findings in this project are publicly available on Zenodo at <https://doi.org/10.5281/zenodo.13623743>. We used R programming language version 4.4.1 (<https://cran.r-project.org/bin/windows/base/>) for all data processing, analysis, and graphical representation.

Submitted 18 October 2024  
Accepted 14 August 2025  
Published 17 September 2025  
10.1126/sciadv.adt9866